Applied Surface Science 528 (2020) 146832

Contents lists available at ScienceDirect

Applied Surface Science

journal homepage: www.elsevier.com/locate/apsusc

Atomistic modeling of energy band alignment in CdTe(1 0 0) and CdTe(1 1 1) surfaces

Anthony P. Nicholson[a,*], Umberto Martinez[b], Akash Shah[a], Aanand Thiyagarajan[a], Walajabad S. Sampath[a]

[a] Next Generation Photovoltaics Center, 1374 Campus Delivery, Fort Collins, CO 80521, USA
[b] Synopsys Denmark ApS, Fruebjergvej 3, DK-2100 Copenhagen, Denmark

ARTICLE INFO

Keywords:
Cadmium telluride
Energy band alignment
Density functional theory
Green's function
Atomistic modeling

ABSTRACT

An atomic-scale perspective of energy band alignment in CdTe surfaces has not been spatially studied despite the major role surfaces play in forming interfaces within CdTe-based thin film photovoltaic devices. Atomistic modeling based on density functional theory coupled with surface Green's function is used for calculating energy band alignment of CdTe surfaces. The CdTe(1 0 0) ((1 × 1) and c(2 × 2) reconstruction) and CdTe(1 1 1) ((1 × 1) and (2 × 2) reconstruction) facets without and with surface relaxation provide insightful band bending characteristics that influence charge carrier transport. Results show that unrelaxed (1 × 1) CdTe(1 0 0) and CdTe (1 1 1) surfaces bend the valence band downward with surface polarity dictating the surface potential magnitude. The reconstructed CdTe(1 0 0) c(2 × 2) and CdTe(1 1 1) (2 × 2) surfaces result in favorable surface electronic features in relation to their unreconstructed variants. In addition, the structurally relaxed CdTe(1 1 1) surfaces develop an internal energy cusp potential that may enhance hole charge transport toward the back of CdTe solar cell devices. Energy band alignments calculated within the study lead to a detailed understanding of how CdTe surfaces may affect CdTe-based thin film photovoltaic applications.

1. Introduction

Electronic properties of surfaces constitute widely recognized features that play a crucial role in thin film semiconductor device physics [1]. By extension, semiconductor surfaces forming junctions within photovoltaic (PV) devices dictate the electronic behaviors of the PV technology as a whole. Thus, as thin film PV devices continue to decrease in size, it is essential to have an atomic-scale perspective that accurately conveys the detailed phenomena associated with thin film PV surfaces.

In the case of cadmium telluride (CdTe) based PV technologies, CdTe surfaces are a critical limiting factor in solar cell efficiencies. Research studies indicate that CdTe surface characteristics dictate minority carrier lifetimes that affect CdTe device performance [2]. However, the relationship between preferential plane orientations of CdTe surfaces, if any exist, to the optimization of junctions within CdTe PV devices are not well understood [3]. CdTe terminated surfaces will exhibit differing polarities depending upon which plane orientation and termination layer (Cd or Te) is examined [4–6]. As a result, various plane orientations of the CdTe surface will influence the electronic properties in the device, especially in areas where interfaces form.

A detailed understanding of the electronic characteristics of CdTe surface plane orientations is essential to the advancement of CdTe device fabrication processes. In this work, atomistic modeling based on Density Functional Theory (DFT) coupled with surface Green's function (SGF) [7] has been utilized for studying the electronic properties found in Cd-terminated CdTe(1 0 0) and (1 1 1) surfaces. Both the unreconstructed and commonly seen reconstructed CdTe surfaces for the (1 0 0) and (1 1 1) plane orientations have been simulated to evaluate the energy band alignment characteristics for each case. The pertinent features calculated in the band alignment diagrams were quantified and compared to understand their effect on carrier charge transport within CdTe-based thin film PV devices.

2. Computational details

The DFT + SGF calculations were performed using the QuantumATK Q-2019.12 software tool [8,9] under a Linear Combination of Atomic Orbitals (LCAO) basis scheme to represent the electronic wavefunctions used to solve the Kohn-Sham eigenvalue problem. A

* Corresponding author.
E-mail address: apnichol@rams.colostate.edu (A.P. Nicholson).

https://doi.org/10.1016/j.apsusc.2020.146832
Received 18 March 2020; Received in revised form 26 May 2020; Accepted 29 May 2020
Available online 10 June 2020
0169-4332/

combination of the FHI and OMX [10,11] pseudopotentials along with their associated double-zeta polarized and low(s2p2d1) basis sets for the respective Cd and Te atoms under the LCAO-DFT methodology were used for all CdTe surface simulations.

A density mesh cutoff of 2200 eV and a doping density of 2×10^{14} cm^{-3} indicative of the intrinsic CdTe p-type carrier concentration were applied in all DFT + SGF modeling cases as well. The k-point density based on a Monkhorst–Pack grid distribution [12] was $3 \times 3 \times 150$ (4.376 Å × 4.376 Å × 154.699 Å) and $4 \times 4 \times 100$ (5.052 Å × 5.052 Å × 178.631 Å) for the CdTe(1 0 0) and (1 1 1) cases, respectively. The Perdew-Zunger form [13] of the LDA exchange–correlation functional was employed in combination with the Hubbard-U correction factor so that appropriate CdTe bulk band gap values could be obtained [14–17] during energy band alignment. The U values within the onsite shell representation were set at 4.60 eV and 2.55 eV for the Cd-4d and Te-5p [16] valence states, respectively, and used throughout the CdTe surface modeling process. The chosen U values allowed for a localized representation of the Cd-4d and Te-5p valence states with energy values that were in good agreement with photoemission spectra measured in other work [18,19].

Fig. 1 depicts the DFT + SGF computational modeling domain (a.k.a. one-probe model) used to represent the CdTe surface during calculations. The one-probe model consists of a bulk electrode that mimics a CdTe periodic structure as a semi-infinite boundary condition for the Green's function formalism. During modeling setup, the CdTe experimental lattice parameter of 6.480 Å [20] is retained in the bulk electrode with the CdTe crystal being cleaved along the plane of interest. This ensures that any effects from relaxation will not significantly impact the convergence of the CdTe band gap set by the Hubbard-U values on the atoms located within the semi-infinite end of the model. The longest part of the model is labeled as the CdTe surface region with length $L_{z,surf}$ where the density matrix iteratively solves for electron density throughout the domain. The region between the CdTe bulk electrode and the CdTe surface region adopted a Dirichlet boundary condition so that the electronic structures of the two regions were coupled together and mimic a semi-infinite bulk region for CdTe. Towards the right of the modeling domain is the vacuum region, which implements a Neumann boundary condition so that the gradient of the electrostatic difference potential with respect to length did not change at the surface (i.e. $d(\delta V)/dr|_{r=L_{z,surf}} = 0$). The one-probe modeling setup ensures that the Poisson solver would accurately converge the electronic structure of each CdTe termination case. The length of the vacuum region $L_{z,vac}$ was kept at 5 nm for all simulation models to maintain consistency in domain lengths. The surface Green's function formalism offers the advantage of better electronic stability with less atomic layers in comparison to the traditional slab model approach [7,21,22].

Cleavage energy calculations for the CdTe(1 0 0) and CdTe(1 1 1)

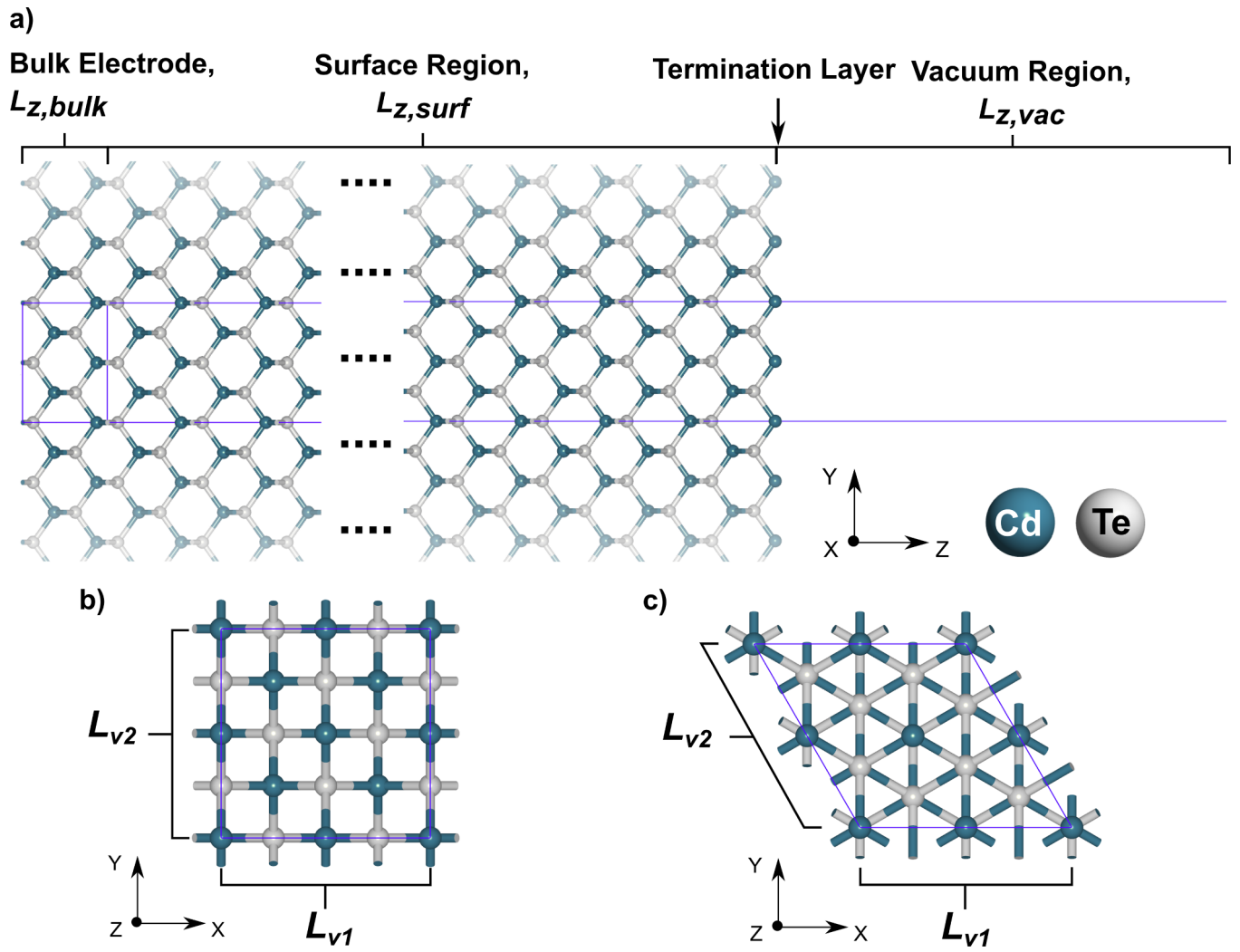

Fig. 1. a) Representation of the CdTe surface one-probe modeling domain. The perimeter of the purple rectangle defines the region that is periodic in the x and y directions. The surface region lengths are provided in Table 1 for reference. b) and c) depict the cross-sections of the (1 0 0) and (1 1 1) plane orientations, respectively, with their edge lengths L_{v1} and L_{v2} both measured at 9.164 Å.

surfaces were performed to quickly verify whether the selected DFT-LCAO parameters were comparable with other studies. The cleavage energy was simply calculated from the DFT + SGF method [7] as follows:

$$\gamma_c = \frac{2E_2 - E_1}{2A} \quad (1)$$

where E_1 is the total energy of the two-probe representation of the CdTe bulk along a given plane orientation, E_2 is the one-probe total energy of the CdTe surface, and A is the cross-sectional area of the simulation domain. The resulting γ_c cleavage energy values were 2.70 and 0.82 J/m^2 for CdTe(1 0 0) and CdTe(1 1 1), respectively, which show that CdTe (1 0 0) has higher surface energetics than CdTe(1 1 1). This is qualitatively in agreement with other cleavage energy calculations from literature [23]. The work presented in this study is mainly focused on the energy band alignment profiles of CdTe surfaces rather than surface energetics. Thus the selected DFT-LCAO parameters were deemed appropriate for well-converged energy band alignment results while maintaining high computational efficiency.

Four different CdTe surface configurations were studied to gain a deeper perspective of the surface properties exhibited by the various Cd-terminated CdTe plane orientations. The (1 × 1) unreconstructed CdTe(1 0 0) and CdTe(1 1 1) surfaces have been experimentally observed for certain deposition/surface treatment conditions [24] and are included in this study. The c(2 × 2) CdTe(1 0 0) (Fig. 2 and (2 × 2) CdTe(1 1 1) (Fig. 3) reconstructed surfaces were created for comparison to their respective unreconstructed counterparts. Both experimental and DFT-based studies have found that these two reconstructed versions of Cd-terminated surfaces were the most thermodynamically stable in epitaxial processes [25–32,19]. The c(2 × 2) CdTe(1 0 0) surface implemented the same periodic cell in the transverse directions as the original (1 × 1) CdTe(1 0 0) surface but required the removal of two Cd atoms from the orginal surface to create it. The periodic cross section of the supercell found in *Li et al.* [29] was adopted for the (2 × 2) CdTe(1 1 1) surface. The main reason for comparing the reconstructed simulations to the unreconstructed ones was to identify the effects on band alignment and surface electronic states due to surface reconstruction. The spatial characteristics for the Cd-terminated unreconstructed vs. reconstructed domains are provided in Table 1. All reconstructed surfaces were created using “ghost” atoms that provide extra LCAO basis functions in the Cd vacancy spots to accurately simulate the surface charge density decay into the vacuum region.

All surface configurations without and with surface relaxation (a.k.a. geometry optimization, GO) applied to them had their electronic properties calculated by the self-consistent field Kohn–Sham method. It was necessary to create modeling groups without and with GO to highlight the important role that GO plays in energy band alignment for Cd-terminated CdTe surfaces. Any effect of CdTe surface relaxation during the deposition process was not known *a priori* but expected to contribute to the overall electronic surface characteristics present on CdTe thin films. Thus, an interatomic force minimization on the surface region extending 5–6 nm from the termination layer was applied to all four CdTe facets of interest to determine how the resulting atomic displacements influenced the energy band alignment. This means that eight unit cells of the CdTe(1 0 0) facets and five unit cells of the CdTe (1 1 1) facets starting from the termination layer underwent GO during the relaxed simulations. All other atoms were fixed to maintain the bulk CdTe band gap value. A force threshold of 0.01 eV/Å was used for all GO surface simulations and compared to the CdTe surfaces without GO. The observed electronic behaviors of CdTe surfaces without and with GO applied give the readers a general outlook on two potential regimes of CdTe surfaces within which most CdTe deposition process conditions are performed. All lengths of the surface domains investigated in the study were made significantly longer than typical one-probe models [7] to account for the band-bending features caused by the screening effects present in the system.

3. Results and discussion

The energy band alignment characteristics and associated relaxation effects that occur on the CdTe(1 0 0) and CdTe(1 1 1) facets were compared to provide key insights on how various CdTe surfaces may affect charge carrier transport. Section 3.1 evaluates the structural characteristics of the CdTe surfaces prior to and after GO is applied to them. Any physical features identified on the CdTe surfaces were used to further explain the energy band alignment features seen in Section 3.2.

3.1. Observations in surface relaxation effects

A number of interesting visual differences are seen between the two CdTe plane orientations. The transition that occurs between Fig. 2a and Fig. 2b shows the dramatic effect that geometry optimization has on the unreconstructed CdTe(1 0 0) surface as the surface deviates from an ordered set of Cd and Te rows. More specifically, the Cd atoms along the horizontal boundaries of the unit cell in the top view of Fig. 2b tend to move toward each other by 1.854 Å. It is notable that the CdTe(1 0 0) surface flattens out with a single Cd atom being displaced 2.794 Å from the topmost relaxed layer. Using the unrelaxed CdTe(1 0 0) atomic positions as a reference, the Cd-termination layer and the Te layer beneath it expand by 0.252 Å and 1.642 Å respectively in the [1 0 0] direction. Similar flattening of the surface due to relaxation is seen between the c (2 × 2) CdTe(1 0 0) surface going from Fig. 2c to Fig. 2d. With the c (2 × 2) unrelaxed case as the reference, the c(2 × 2) CdTe(1 0 0) surface slightly expands by 0.086 Å with the Te layer beneath it expanding by 1.713 Å. The observed relaxation effect is due to the removal of two Cd atoms from the termination layer and at least for the c(2 × 2) case has been observed in other DFT-based studies [33,27]. It must be noted that the relaxation procedure as well as the one-probe surface setup in the present work lead to different values for the c(2 × 2) CdTe(1 0 0) atomic positions in the [1 0 0] direction. However, the quantitative differences may also be attributed to the greater relaxation region used in the present work. Nonetheless, the two Cd vacancies lead to a rearrangement of charge that causes the underlying Te layer to expand in the [1 0 0] direction to compensate the effect. The preferred undimerized flat structure obeys the Electron Counting Rule (ECR) for the Cd-terminated c(2 × 2) CdTe(1 0 0) surface [25,27] since the number of empty cation (Cd) dangling bonds is equal to the number of fully occupied anion (Te) dangling bonds. As a result, the dramatic relaxation effects observed in the CdTe(1 0 0) unreconstructed and reconstructed surfaces directly influence the energy band alignment diagrams and their associated surface electronic states as presented in Section 3.2.

Regarding the CdTe(1 1 1) plane orientations, Fig. 3 provides a clear indication that the (2 × 2) surface reconstruction is the energetically minimized facet. This is validated by the fact that after the original CdTe(1 1 1) unrelaxed surface in Fig. 3a undergoes relaxation, a single Te atom is displaced 2.899 Å from its original position in the [111] direction. After relaxation, the CdTe(1 1 1) (1 × 1) surface tends to have Te atoms residing closer to the surface. The atomic displacements of the relaxed surface lead to the force-minimized cross-section found in Fig. 3b, which appears to be quite disordered in relation to its unrelaxed state. On the other hand, the (2 × 2) CdTe(1 1 1) facet before and after relaxation as seen in Fig. 3c and Fig. 3d, respectively, maintains a well-behaved surface arrangement along the cross-sectional view due to the Cd vacancy. Most of the atoms in the topmost Cd layer of the CdTe (1 1 1) (1 × 1) surface minimally compress by 0.174 Å while the underlying Te layer expands by 0.808 Å in the [111] direction. For the CdTe(1 1 1) (2 × 2) surface, the compressive and tensile displacements for the Cd and Te topmost layers are 0.471 Å and 0.557 Å, respectively. Qualitatively, the resulting displacements and formation of flat CdTe (1 1 1) surfaces are in agreement with other calculations [29,34]. Again, the explanation for the resulting planar surface leads back to the (2 × 2) CdTe(1 1 1) surface obeying the ECR in a similar manner as the III-V semiconducting compounds [35,36]. Within the cross-sectional

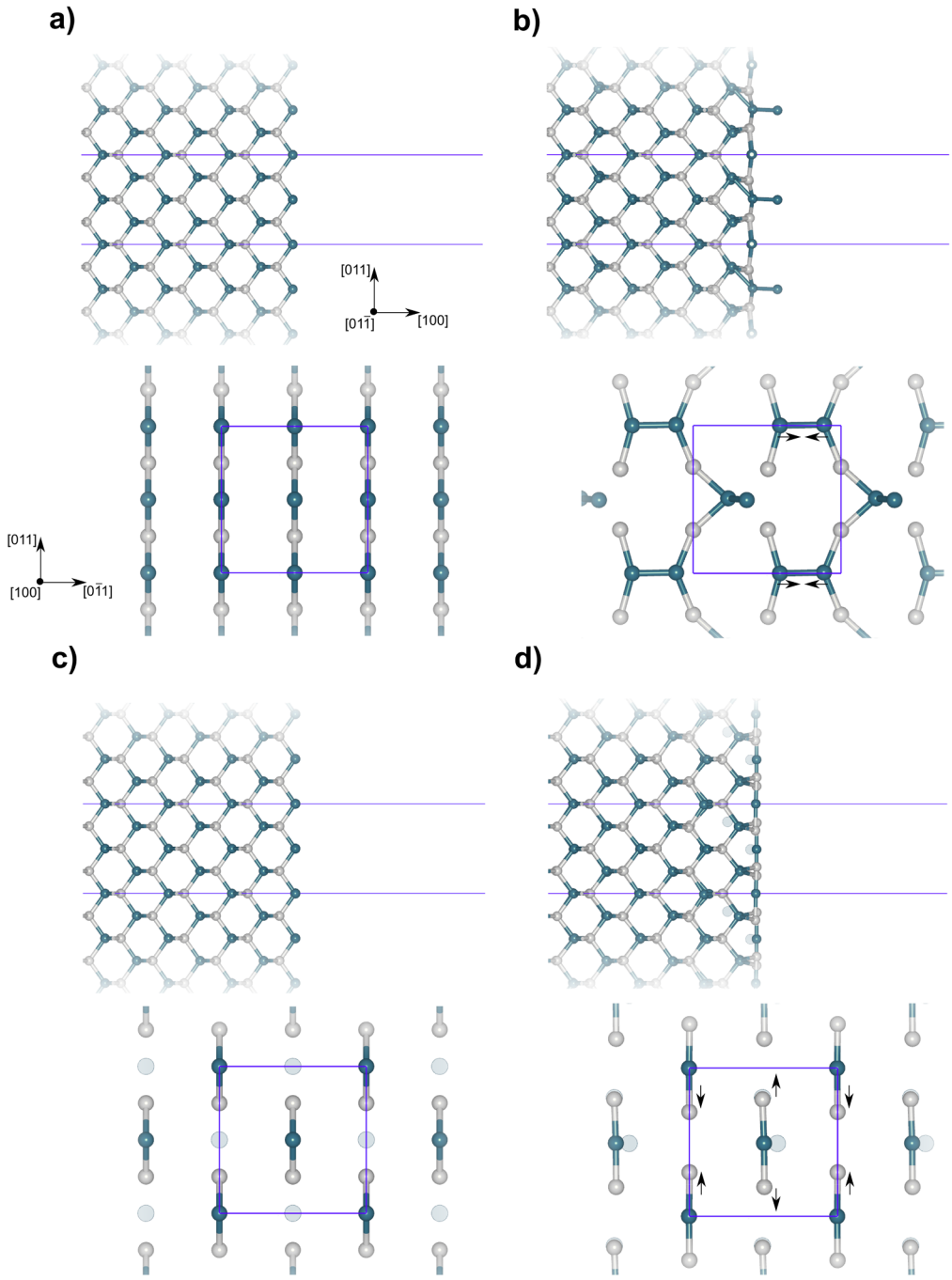

Fig. 2. Perspective views of the respective unrelaxed and relaxed atomic configurations of (a,b) the (1 × 1) unreconstructed and (c,d) the c(2 × 2) reconstructed CdTe(1 0 0) surfaces. Two views are shown along the transport direction (top subfigure) and perpendicular directions (bottom subfigure) of the one-probe models. The perpendicular view only shows the last two atomic layers in the surface domain for clarity. All surfaces are visualized using the indices provided in (a). The "ghost" atoms are shown as translucent circles in (c, d).

unit cell of the unreconstructed CdTe(1 1 1) surface, there are an equal number of cations and anions present, each of which exhibit sp^3 orbital hybridization. After removing one Cd atom, each of the three underlying Te atoms that were bonded to the Cd atom are left with occupied dangling bonds. Geometry optimization of the (2 × 2) CdTe(1 1 1) surface allows for atomic layers to shift accordingly to ensure the surface maintains charge neutrality. Thus, the underlying Te layer moves closer to the Cd termination layer, causing the three occupied dangling bonds from Te to be eliminated by the empty dangling bonds from the remaining three Cd surface atoms in the cross-sectional unit cell. The (2 × 2) CdTe(1 1 1) surface has been observed experimentally over a wide temperature range [32], proving its stability as the favorable facet for the CdTe(1 1 1) cases.

3.2. Investigation of energy band alignment and surface state characteristics

Local density of states projected along the direction perpendicular to the surface plane of the CdTe surfaces were plotted to describe the energy band alignment features for a given Cd-terminated surface of CdTe. Relevant electronic characteristics measured from the energy band alignment plots such as band gap energy $E_{g,CdTe}$, surface energy potential E_{surf}, and internal cusp energy potential E_{cusp} (if any exists)

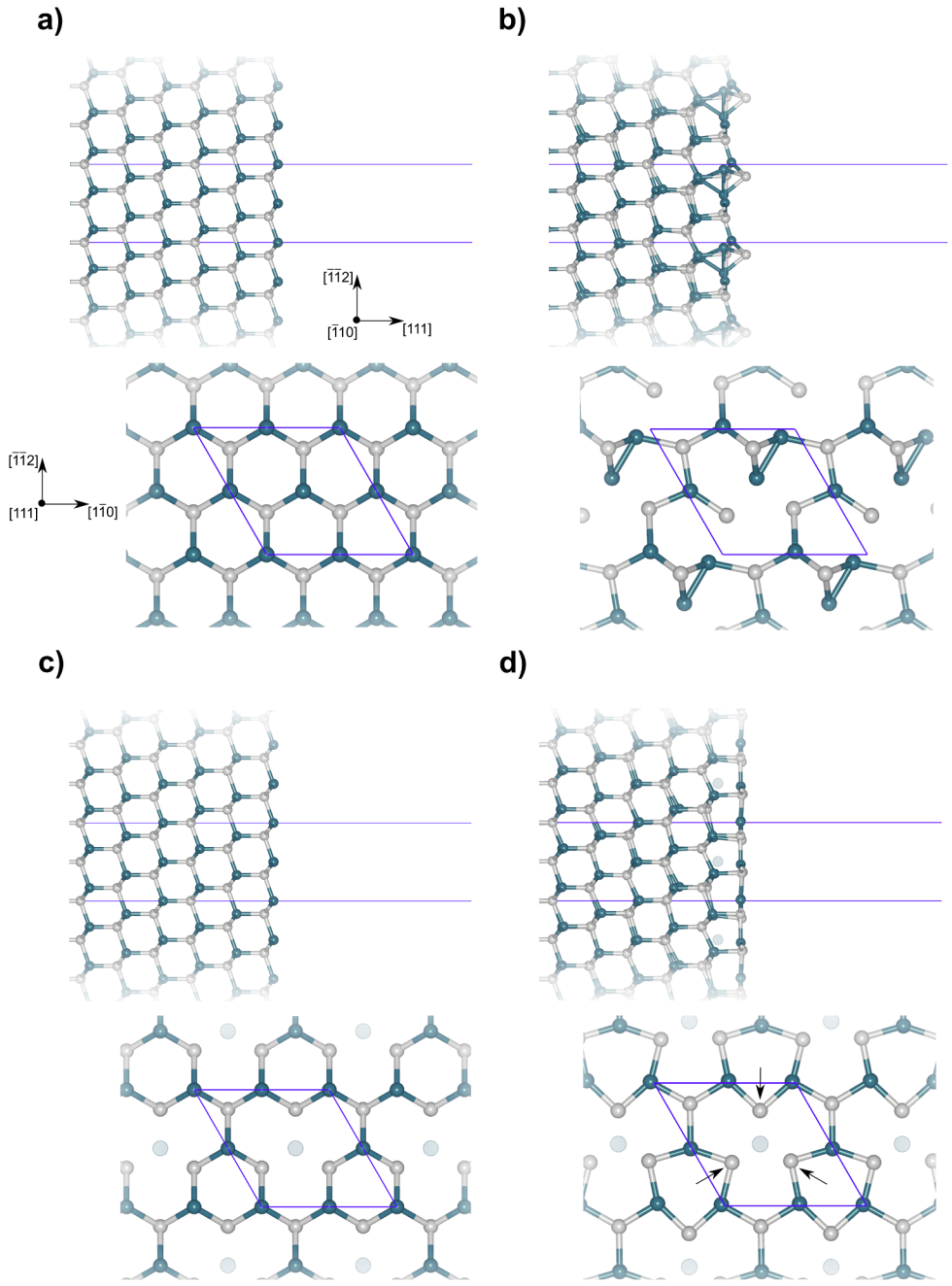

Fig. 3. Perspective views of the respective unrelaxed and relaxed atomic configurations of (a,b) the (1 × 1) unreconstructed and (c, d) the (2 × 2) reconstructed CdTe(1 1 1) surfaces. Two views are shown along the transport direction (top subfigure) and perpendicular directions (bottom subfigure) of the one-probe models. The perpendicular view only shows the last two atomic layers in the surface domain for clarity. All surfaces are visualized using the indices provided in (a). The "ghost" atoms are shown as translucent circles in (c, d).

were reported in Table 2 for the (1 0 0) and (1 1 1) CdTe surfaces. The two most prominent surface electronic state energy levels (E_{def1} and E_{def2}, respectively) as well as their DOS magnitudes ($D(E_{def1})$ and $D(E_{def2})$, respectively) were tabulated in Table 3.

A standard for measuring electronic features such as the CdTe band gap, surface and internal cusp energy potentials was established by using macroscopically averaged curve fits of the valence band maximum (VBM) and conduction band minimum (CBM) with a Gaussian kernel width of 5 Å. The Gaussian kernel width was chosen so that the curve fits for VBM/CBM would minimize the oscillatory effects of tracing between alternating Cd and Te layers. Too large of a width value resulted in the shrinking of the curve fits as wider Gaussian widths required more data slices to smoothen the curve traces. Furthermore, a DOS threshold of 10^{-4} eV^{-1} was selected as done in another DFT-LCAO study [37] to distinguish between the band edges and background noise during the tracing process.

Using the macroscopically averaged curve fits of the VBM and CBM, the band gap energy $E_{g,CdTe}$ was consistently determined from the energy differences of the VBM and CBM at positions located closest to the bulk-like CdTe electrode region (the leftmost part of each surface region). The Hubbard-U values described in Section 2 have accurately described the energy band gap values for the CdTe bulk electrodes to ensure transferability in the one-probe modeling setup.

In the context of the macroscopically averaged curve fit for the

Table 1
CdTe one-probe modeling dimensions of the bulk electrode and surface regions for various plane orientations and surface reconstructions. The subscripts "u" and "r" denote the unrelaxed and relaxed domain lengths of the CdTe surface models. N_{bulk} and N_{surf} represent the number of physical atoms ("ghost" atoms omitted) within the bulk and surface regions, respectively.

	(1 0 0)		(1 1 1)	
	(1 × 1)	c(2 × 2)	(1 × 1)	(2 × 2)
$L_{z,bulk}$ (Å)	6.480	6.480	11.224	11.224
$L_{z,surf(u)}$ (Å)	213.030	213.030	223.071	223.071
$L_{z,surf(r)}$ (Å)	215.827	213.116	225.034	222.281
N_{surf}	528	526	480	479
N_{bulk}	16	16	24	24

VBM, the surface potential E_{surf} is defined as the energy difference between the VBM curve fit value nearest the surface and the curve fit VBM value of the CdTe bulk-like region. Both of the specified locations are respectively labeled as points 1 and 2 in Fig. 4a. Depending on whether it bends upward or downward, E_{surf} acts as either a barrier (negative magnitude, bending downward) or an enhancer (positive magnitude, bending upward) for hole transport toward the back of a typical p-type CdTe PV device. In accordance with the labels provided in Fig. 5c, the cusp energy potential E_{cusp} is simply defined as the energy difference between the peak of the curve fit VBM (labeled point 1) and the leftmost part of the same curve fit (labeled point 2). The length δ_{cusp} marks the position where the cusp energy potential begins with respect to the surface region length $L_{z,surf}$.

The two surface states with the highest DOS magnitudes were recorded as E_{def1} and E_{def2} in Table 3 and were measured within 5 Å from the termination layer. This was done to maintain consistency with where the most prominent surface electronic states were evaluated in each modeling case.

3.2.1. CdTe(1 0 0) terminated surfaces

Fig. 4 shows the energy band alignment of the respective CdTe (1 0 0) one-probe models. As shown in Table 2, the band gap energies $E_{g,CdTe}$ for the CdTe(1 0 0) configurations lie between 1.47 eV and 1.50 eV, in agreement with the experimental value of 1.49 eV [38]. Fig. 4a and b are the respective unrelaxed and relaxed one-probe results for the (1 × 1) CdTe(1 0 0) surface. Fig. 4c and Fig. 4d are the respective unrelaxed and relaxed band alignment analyses corresponding to the c (2 × 2) CdTe(1 0 0) surface.

In the CdTe(1 0 0) unrelaxed case without reconstruction (Fig. 4a), a shallow downward bend of −0.14 eV in the valence band forms while negligible band bending occurs in the conduction band. The valence band bending presents a barrier to the hole majority charge carriers that would lead to a decreased efficiency if all band alignment features at the back of the absorber layer were maintained in a complete CdTe device. Furthermore, a large range of surface state levels extending both above and below the Fermi level E_F appear at the CdTe(1 0 0) surface. The two biggest DOS magnitudes for the surface states in the one-probe model exist at +0.07 and +0.01 eV from the Fermi level. Surface electronic states closer to the Fermi level, at least from a first-order perspective, are potential avenues for Shockley Read Hall recombination within a CdTe device if the features were retained at the back of an equivalent CdTe(1 0 0) absorber layer. However, detrimental features are seen in the energy band alignment profile when GO is introduced to the (1 × 1) CdTe(1 0 0) surface. The relaxed surface shown in Fig. 4b continues to have a downward valence band bend but now contains a wider range of surface state levels. It is evident that within the present modeling setup the relaxation effects actually worsen the surface states characteristics for the CdTe(1 0 0) (1 × 1) case. It is worth mentioning that the entire screening length of the CdTe(1 0 0) (1 × 1) surface is not fully accomodated, which is why the VBM does not flatten out near the CdTe bulk region. One way to alleviate the bend would be with a higher doping concentration than the 2×10^{14} cm^{-3} value used in the current work. However, a lower doping concentration was used to reflect typical concentrations seen within intrinsic CdTe PV devices. In any case, the CdTe(1 0 0) (1 × 1) surface leads to unfavorable surface states and downward VBM bending that are harmful to hole carrier transport toward the back of p-type CdTe solar cell devices.

The CdTe(1 0 0) c(2 × 2) surface band alignment depicted in Fig. 4c provides several noteworthy differences from the unreconstructed case. First, the valence band has a gradual upward bend of + 0.28 eV as oppose to the negative downward bend seen in CdTe(1 0 0) valence band. By extension, the conduction band also slightly bends upward, which was not observed for the CdTe(1 0 0) (1 × 1) surface. The surface states levels E_{def1} and E_{def2} for CdTe(1 0 0) c(2 × 2) reside at least + 0.50 eV above the Fermi level E_F in a concentrated manner rather than throughout the energy gap. The concentrated DOS of the surface electronic states is primarily due to the remaining Cd atoms at the CdTe (1 0 0) termination layer after creating two Cd vacancies. Since no GO has been applied to the surface yet, charge compensation has not been achieved along the CdTe(1 0 0) c(2 × 2) surface and leads to the features seen in Fig. 4c. Once GO is performed on the CdTe(1 0 0) c(2 × 2) facet, a flattening of the bands is achieved as shown in Fig. 4d due to the force-minimized atomic displacements. As mentioned in 3.1, relaxation of the CdTe(1 0 0) c(2 × 2) surface into an undimerized, charge neutral surface leads to the fulfillment of the electron counting model. Along this facet, the surface energy potential E_{surf} of −0.03 eV is both smaller and opposite in sign from the + 0.28 eV surface potential found in the unrelaxed case. However, the surface states above the Fermi level have virtually disappeared as both surface states in Table 3 have a DOS magnitude of 10^{-4} eV^{-1}. The second surface state at −0.96 eV nearest the termination layer resides below the measured bulk VB for CdTe. This is simply due to the chosen Gaussian width of the macroscopic curve fit only tracing close to the surface based on how the Gaussian kernel is set up for averaging the VBM. A newly formed cusp energy potential with a small magnitude E_{cusp} of + 0.05 eV is

Table 2
Salient electronic features within each (1 0 0) and (1 1 1) CdTe one-probe model. δ_{cusp} indicates the position where the cusp energy potential E_{cusp} is determined starting from the termination layer. All energy band alignment values are determined from the macroscopically averaged curve fit of each local density of states plot. Any +/- values indicate energy values referenced to the Fermi level E_F (marked as 0 eV).

Type	Facet	$E_{g,CdTe}$ (eV)	E_{surf} (eV)	δ_{cusp} (Å)	E_{cusp} (eV)
Unrelaxed	$CdTe(1\,0\,0)_{(1\times1)}$	1.49	−0.14	n/a	n/a
	$CdTe(1\,0\,0)_{c(2\times2)}$	1.47	+0.28	n/a	n/a
	$CdTe(1\,1\,1)_{(1\times1)}$	1.48	−0.38	n/a	n/a
	$CdTe(1\,1\,1)_{(2\times2)}$	1.47	+0.01	n/a	n/a
Relaxed	$CdTe(1\,0\,0)_{(1\times1)}$	1.49	−0.15	n/a	n/a
	$CdTe(1\,0\,0)_{c(2\times2)}$	1.50	−0.03	51.926	+0.05
	$CdTe(1\,1\,1)_{(1\times1)}$	1.40	+0.09	59.017	+0.33
	$CdTe(1\,1\,1)_{(2\times2)}$	1.46	−0.02	63.746	+0.07

Table 3
Surface electronic state energy levels and DOS magnitudes within each (1 0 0) and (1 1 1) CdTe one-probe model. All electronic state energy values for a given facet are chosen according to highest DOS magnitude and are accurate to within ±5 meV.

Type	Facet	E_{def1} (eV)	$D(E_{def1})$ (eV^{-1})	E_{def2} (eV)	$D(E_{def2})$ (eV^{-1})
Unrelaxed	$CdTe(100)_{(1 \times 1)}$	+0.07	2.56×10^{-1}	+0.01	2.07×10^{-1}
	$CdTe(100)_{c(2 \times 2)}$	+0.61	1.47×10^{2}	+0.56	4.44×10^{-1}
	$CdTe(111)_{(1 \times 1)}$	+0.23	6.48×10^{-1}	−0.40	2.60×10^{-1}
	$CdTe(111)_{(2 \times 2)}$	−0.81	9.73×10^{-3}	−0.80	4.74×10^{-3}
Relaxed	$CdTe(100)_{(1 \times 1)}$	+0.62	5.98×10^{1}	−0.30	2.45×10^{1}
	$CdTe(100)_{c(2 \times 2)}$	+0.68	6.69×10^{-4}	−0.96	2.47×10^{-4}
	$CdTe(111)_{(1 \times 1)}$	+0.56	6.80×10^{-2}	+0.67	4.72×10^{-2}
	$CdTe(111)_{(2 \times 2)}$	+0.62	7.55×10^{-2}	+0.65	1.05×10^{-2}

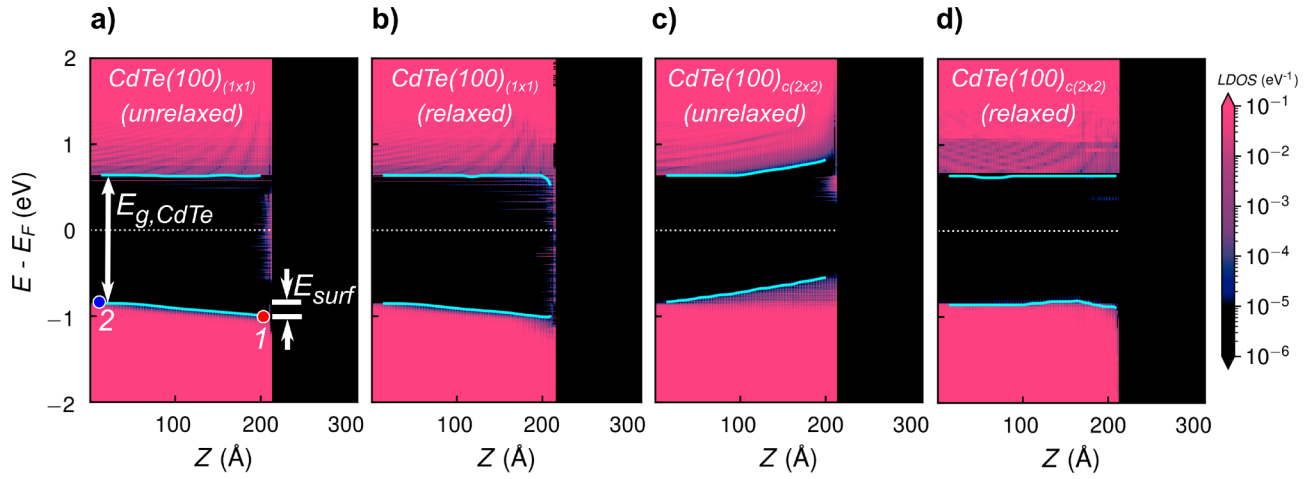

Fig. 4. Localized density of states mapping across the unreconstructed and reconstructed CdTe(1 0 0) one-probe models separated as unrelaxed (a, c) and relaxed cases (b, d). Plane orientation and reconstruction type are provided in each image above. The zero energy on the y-axis is referenced by the Fermi level E_F of each respective band alignment profile. The light blue curves are the macroscopically averaged curve fits of the valence band maximum and conduction band minimum, respectively. Points 1 and 2 in (a) are used to determined the surface energy potential E_{surf} with details provided in Section 3.2.

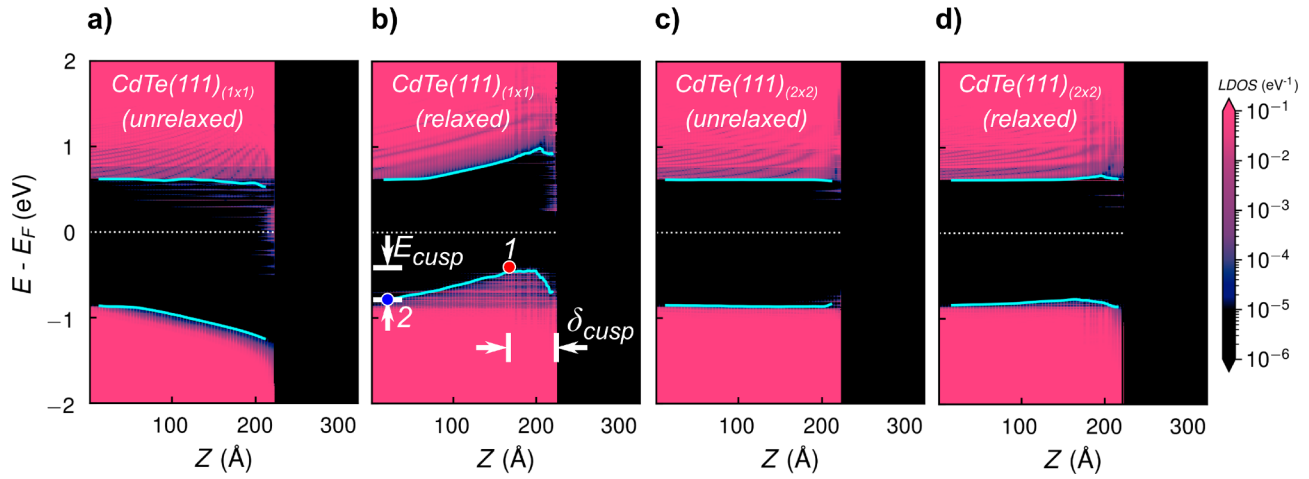

Fig. 5. Localized density of states mapping across the unreconstructed and reconstructed CdTe(1 1 1) one-probe models separated as unrelaxed (a, b) and relaxed cases (c, d). Plane orientation and reconstruction type are provided in each image above. The zero energy on the y-axis is referenced by the Fermi level E_F of each respective band alignment profile. The light blue curves are the macroscopically averaged curve fits of the valence band maximum and conduction band minimum, respectively. Points 1 and 2 in (b) are used to determined the cusp energy potential E_{cusp} with details provided in Section 3.2.

created only for the CdTe(1 0 0) c(2 × 2) case. In terms of charge transport, this shallow energy feature should not significantly impede or enhance carrier flow. Several pertinent characteristics of the CdTe (1 0 0) c(2 × 2) unrelaxed surface are changed by the applied relaxation to its surface. It is clear that relaxation of the CdTe(1 0 0) plane oriented surfaces has a strong effect on the band alignment features present at the surface.

In accordance with surface polarity, CdTe(1 0 0) plane orientations can be classified as macroscopically non-polar surfaces if demi-steps (A to B facet steps) are considered [5]. However, the current atomistic modeling on CdTe(1 0 0) surfaces will have some type of charging effect present that causes the bands to bend as a polar surface. Only the c (2 × 2) reconstruction after relaxation was able to have flatter bands with minimal surface electronic states as it satisfies the ECR. It is

therefore evident that a relaxed reconstructed c(2 × 2) CdTe(1 0 0) surface provides the most favorable conditions out of the CdTe(1 0 0) cases studied for hole carrier transport in CdTe PV devices.

3.2.2. CdTe(1 1 1) terminated surfaces

As shown in Fig. 5, two different CdTe(1 1 1) surfaces were investigated for comparison to each other as well to the CdTe(1 0 0) plane orientations described in Section 3.2.1. Fig. 5a and Fig. 5b depict the energy band alignment features present for the unrelaxed and relaxed cases, respectively, for the (1 × 1) CdTe(1 1 1) surface. Fig. 5c and Fig. 5d represent the unrelaxed and relaxed cases, respectively, for the (2 × 2) CdTe(1 1 1) surface reconstruction. All electronic properties obtained from the band profiles of each CdTe(1 1 1) one-probe model are quantified in Tables 2 and 3. An investigation of the CdTe(1 1 1) surfaces provides direct insights on how plane orientation affects energy band alignment properties from a spatial representation across the surface domain.

Band alignment for the unrelaxed CdTe(1 1 1) (1 × 1) surface is presented in Fig. 5a. As in the CdTe(1 0 0) case, the CdTe(1 1 1) surface displays a downward valence band bending of −0.38 eV with several shallow surface states that extend far into the surface region (~ 10 nm). The conduction band remains relatively flat as the surface states are discretely spaced out across the energy band gap of the rightmost part of the surface region. As in the CdTe(1 0 0) configuration, the surface electronic states could potentially increase carrier recombination as seen with E_{def1} (+0.23 eV) and E_{def2} (-0.40) surface states levels with 10^{-1} eV^{-1} DOS magnitudes. After relaxing the CdTe(1 1 1) unreconstructed surface, the surface states shift further above E_F with an order of magnitude smaller DOS value. Yet, the most intrigue detail of energy band alignment along the respective facet was discovered. The relaxed CdTe(1 1 1) (1 × 1) case in Fig. 5b no longer has a large downward valence bend but instead has developed a large cusp energy potential E_{cusp} with a height of 0.33 eV. The resulting cusp feature has been recognized within CdTe PV devices such as the CdTe/Te interface by means of a photoelectron spectroscopy characterization study performed by *Fritsche et al.* [38]. The study demonstrates a hole enhancing feature that resides near the CdTe/Te interface to facilitate hole transport toward the back of the PV device. Furthermore, a similar cusp energy potential height was obtained for the computational study of CdTe(1 1 1)/Te [39] that only occurs after relaxation of the CdTe(1 1 1) surface. It must be stated the experimental study by *Fritsche et al.* was done for polycrystalline CdTe while the results in the current work are for a pristine (1 1 1) oriented CdTe single crystal surface. Nonetheless, it is suggested that the geometry optimized, unreconstructed CdTe(1 1 1) surface can provide an additional mechanism for hole transport that is not seen in the CdTe(1 0 0) cases.

Looking at the CdTe(1 1 1) reconstructed case in Fig. 5c, the CdTe (1 1 1) (2 × 2) surface has a negligible valence band bending effect (E_{surf} = +0.01 eV) than its unreconstructed counterpart. Furthermore, the surface states levels have decreased appreciably with the highest concentration of surface states being nearly −0.80 eV below E_F. The unrelaxed CdTe(1 1 1) (2 × 2) surface shows distinct differences in band bending and surface states from the (1 × 1) unreconstructed case that establishes the role of Cd surface vacancies for polarized CdTe facets. After GO is achieved on the CdTe(1 1 1) (2 × 2) surface as shown in Fig. 5d, an energy potential cusp develops with a magnitude E_{cusp} = +0.07 eV above the valence band of the bulk CdTe region. The cusp energy potential occurs δ_{cusp} = 63.746 Å from the Cd-termination layer of the CdTe(1 1 1) (2 × 2) one-probe model, which is similar to the CdTe(1 1 1) (1 × 1) cusp location at 59.017 Å. The δ_{cusp} value is within the region length that has been structurally relaxed (GO ~ 5–6 nm) in the CdTe(1 1 1) surface. Therefore, the spatial position of the cusp energy potential E_{cusp} for both the relaxed cases of the unreconstructed and reconstructed CdTe(1 1 1) one-probe models correlates with the GO size used to minimize the atomic forces. Similar to the CdTe(1 0 0) c (2 × 2) case, the (2 × 2) surface reconstruction also mitigates the CdTe surface recombination limiting factor brought upon by surface elecronic states since the CdTe(1 1 1) (2 × 2) surface obeys the ECR as described in Section 3.1. It is clear that the CdTe(1 1 1) (2 × 2) surface decreases the electronic states that were present in the (1 × 1) relaxed case and still develops a small energy cusp.

The energy cusp in both the CdTe(1 1 1) (1 × 1) and (2 × 2) cases provides a new insight in band alignment that is strictly dependent on the plane orientation and the amount of relaxation present in the CdTe surface. Although a small energy cusp was seen for the CdTe(1 0 0) c (2 × 2) case, the cusp seen specifically for the CdTe(1 1 1) (1 × 1) case has a greater magnitude and thus would lead to better majority charge carrier (holes) transport at the back of a CdTe device. Two possibilities to create the same cusp potentials seen in either Fig. 5c or Fig. 5d for improved hole current transport in a CdTe(1 1 1) absorber layer are proposed as follows: 1) develop a CdTe deposition process that relaxes the CdTe(1 1 1) (1 × 1) or (2 × 2) surface less than 5 nm from the termination layer; 2) fabricate a CdTe(1 1 1) facet that relaxes 5 nm within the surface but undergoes some type of etching process that extends past the downward valence band bend while retaining $E_{cusp} > E_{V,CdTe}$. The energy cusp readily seen in (1 1 1) but minimized in (1 0 0) CdTe surfaces reveals the importance of plane orientation and surface relaxation as some of the possible mechanisms leading to improved CdTe PV device performance.

4. Conclusion

The DFT + SGF approach to investigating the electronic features of the CdTe surface gives a detailed picture of atomic-scale electronic behaviors that cannot be studied from surface theory and classical band alignment models alone. Atomistic modeling of CdTe(1 0 0) and CdTe (1 1 1) oriented facets reveals the importance of plane orientation, surface reconstruction, and surface relaxation to the determination of electronic behaviors in CdTe surfaces.

There is a complex relationship between electronic performance of CdTe to its plane orientation. Both the (1 0 0) and (1 1 1) CdTe surfaces lead to a unique description of the band bending profile that adds to the conventional understanding of CdTe surface polarity. In general, the Cd-termination layer bends downward with surface polarity determining the amount of bending as suggested in surface theory [40]. Geometric optimization leads to key insights on how relaxed CdTe surfaces distribute charge densities that introduce vastly different energy band profiles than the unrelaxed cases. For most of the CdTe relaxed variants, the surface electronic states are reduced by the minimization of atomic forces that may mitigate recombination losses at the CdTe surface.

The investigation of unreconstructed vs. reconstructed CdTe surfaces within their respective plane orientations provide strong conclusions. In general, the reconstructed surfaces give the most favorable structural and electronic characteristics that lead to cleaner CdTe energy band alignments. Both the CdTe(1 0 0) c(2 × 2) and CdTe(1 1 1) (2 × 2) reconstructed surfaces obey the ECR that leads to charge compensated surfaces and thus virtually no surface electronic states. The superiority of reconstructed CdTe surfaces indicates how the surface point defects considered in the study are beneficial along their respective plane orientations.

The most prominent feature seen exclusively for the relaxed CdTe (1 1 1) surfaces is the favorable energy cusp that forms within the surface band profile. The resulting cusp feature has been recognized at the CdTe/Te interface (albeit a polycrystalline CdTe layer) with a photoelectron spectroscopy characterization study performed by *Fritsche et al.* [38]. Furthermore, a previous computational study on the CdTe(1 1 1)/Te interface indicates a similar cusp feature existing within the unreconstructed CdTe(1 1 1) region [39]. If the cusp feature along the CdTe(1 1 1) plane orientation could be retained throughout the CdTe fabrication process, it may provide an additional mechanism for improving hole carrier transport in CdTe PV devices.

The detailed aspects revealed in the DFT + SGF modeling approach of CdTe(1 0 0) and (1 1 1) facets give a fundamental overview of electronic features in CdTe surfaces. Energy band alignment from an atomistic computational standpoint enables the understanding of CdTe surfaces without the reliance on pre-determined band alignment properties required in theoretical models such as the Anderson Rule [41]. In turn, the spatial characteristics obtained from the DFT + SGF CdTe surface models can later be verified by surface and near-interface characterization techniques such as photoelectron spectroscopy and time-resolved photoluminescence. The atomistic perspectives of CdTe surfaces provide further guidance for deposition processes to be modified so as to achieve optimal CdTe surface properties used in CdTe-based thin film PV applications.

CRediT authorship contribution statement

Anthony P. Nicholson: Conceptualization, Methodology, Software, Validation, Formal analysis, Investigation, Data curation, Writing - original draft, Visualization. **Umberto Martinez:** Software, Writing - review & editing, Supervision. **Akash Shah:** Software, Formal analysis, Data curation, Writing - review & editing. **Aanand Thiyagarajan:** Software, Formal analysis, Data curation, Writing - review & editing. **Walajabad S. Sampath:** Conceptualization, Resources, Project administration, Funding acquisition.

Declaration of competing interest

The authors declare that they have no known competing financial interests or personal relationships that could have appeared to influence the work reported in this paper.

Acknowledgements

The authors would like to thank Dr. Chris Weinberger and Dr. Ken Durose for their timely insight and suggestions regarding surface energetics and surface polarities of CdTe plane orientations. This material is based upon work supported by the National Science Foundation Graduate Research Fellowship Program under Grant No. DGE-1321845, INTERN Program under Grant No. 1540007, and Industry-University Cooperative Research Centers Program under Grant No. 1821526. Any opinions, findings, and conclusions or recommendations expressed in this material are those of the author(s) and do not necessarily reflect the views of the National Science Foundation. This work utilized the Summit supercomputer, which is supported by the National Science Foundation (awards ACI-1532235 and ACI-1532236), the University of Colorado Boulder, and Colorado State University. The Summit supercomputer is a joint effort of the University of Colorado Boulder and Colorado State University.

References

[1] R.H. Williams, Surface defects on semiconductors, Surf. Sci. 132 (1) (1983) 122–142, https://doi.org/10.1016/0039-6028(83)90535-6.
[2] M.O. Reese, C.L. Perkins, J.M. Burst, S. Farrell, T.M. Barnes, S.W. Johnston, D. Kuciauskas, T.A. Gessert, W.K. Metzger, Intrinsic surface passivation of CdTe, J. Appl. Phys. 118 (15) (2015), https://doi.org/10.1063/1.4933186 155305.
[3] R. Scheer, H.-W. Schock, Chalcogenide Photovoltaics: Physics, Technologies, and Thin Film Devices, Wiley-VCH John Wiley distributor, Weinheim Chichester, 2011.
[4] E.P. Warekois, M.C. Lavine, A.N. Mariano, H.C. Gatos, Crystallographic Polarity in the II–VI Compounds, J. Appl. Phys. 33 (2) (1962) 690–696, https://doi.org/10.1063/1.1702489.
[5] D.B. Holt, Surface polarity and symmetry in semiconducting compounds, J. Mater. Sci. 23 (3) (1988) 1131–1136, https://doi.org/10.1007/BF01154024.
[6] P. Brown, K. Durose, G.J. Russell, J. Woods, The absolute determination of CdTe crystal polarity, J. Cryst. Growth 101 (1) (1990) 211–215, https://doi.org/10.1016/0022-0248(90)90968-Q.
[7] S. Smidstrup, D. Stradi, J. Wellendorff, P.A. Khomyakov, U.G. Vej-Hansen, M.-E. Lee, T. Ghosh, E. Jónsson, H. Jónsson, K. Stokbro, First–principles Green's-function method for surface calculations: a pseudopotential localized basis set approach, Phys. Rev. B 96 (2017), https://doi.org/10.1103/PhysRevB.96.195309 195309.
[8] S. Smidstrup, T. Markussen, P. Vancraeyveld, J. Wellendorff, J. Schneider, T. Gunst, B. Verstichel, D. Stradi, P.A. Khomyakov, U.G. Vej-Hansen, M.-E. Lee, S.T. Chill, F. Rasmussen, G. Penazzi, F. Corsetti, A. Ojanperä, K. Jensen, M.L.N. Palsgaard, U. Martinez, A. Blom, M. Brandbyge, K. Stokbro, QuantumATK: an integrated platform of electronic and atomic-scale modelling tools, J. Phys. Condens. Matter 32 (1) (2019), https://doi.org/10.1088/1361-648x/ab4007 015901.
[9] QuantumATK Q-2019.12, Synopsys QuantumATK.
[10] T. Ozaki, Variationally optimized atomic orbitals for large-scale electronic structures, Phys. Rev. B 67 (2003), https://doi.org/10.1103/PhysRevB.67.155108 155108.
[11] T. Ozaki, H. Kino, Numerical atomic basis orbitals from H to Kr, Phys. Rev. B 69 (2004), https://doi.org/10.1103/PhysRevB.69.195113 195113.
[12] H.J. Monkhorst, J.D. Pack, Special points for Brillouin-zone integrations, Phys. Rev. B 13 (1976) 5188–5192, https://doi.org/10.1103/PhysRevB.13.5188.
[13] J.P. Perdew, A. Zunger, Self-interaction correction to density-functional approximations for many-electron systems, Phys. Rev. B 23 (1981) 5048–5079, https://doi.org/10.1103/PhysRevB.23.5048.
[14] S. Lalitha, S. Karazhanov, P. Ravindran, S. Senthilarasu, R. Sathyamoorthy, J. Janabergenov, Electronic structure, structural and optical properties of thermally evaporated CdTe thin films, Physica B Condens. Matter 387 (1) (2007) 227–238, https://doi.org/10.1016/j.physb.2006.04.008.
[15] M. Aras, Ç. Kılıç, Combined hybrid functional and DFT + U calculations for metal chalcogenides, J. Chem. Phys. 141 (4) (2014), https://doi.org/10.1063/1.4890458 044106.
[16] P. Gopal, M. Fornari, S. Curtarolo, L.A. Agapito, L.S.I. Liyanage, M.B. Nardelli, Improved predictions of the physical properties of Zn- and Cd-based wide band-gap semiconductors: a validation of the ACBN0 functional, Phys. Rev. B 91 (2015), https://doi.org/10.1103/PhysRevB.91.245202 245202.
[17] Y. Wu, G. Chen, Y. Zhu, W.-J. Yin, Y. Yan, M. Al-Jassim, S.J. Pennycook, LDA + U/GGA + U calculations of structural and electronic properties of CdTe: dependence on the effective U parameter, Comput. Mater. Sci. 98 (2015) 18–23, https://doi.org/10.1016/j.commatsci.2014.10.051.
[18] D.W. Niles, X. Li, P. Sheldon, H. Høchst, A photoemission determination of the band diagram of the Te/CdTe interface, J. Appl. Phys. 77 (9) (1995) 4489–4493, https://doi.org/10.1063/1.359444.
[19] J. Ren, L. Fu, G. Bian, M. Wong, T. Wang, G. Zha, W. Jie, T. Miller, M.Z. Hasan, T.-C. Chiang, Spectroscopic studies of CdTe(1 1 1) bulk and surface electronic structure, Phys. Rev. B 91 (2015), https://doi.org/10.1103/PhysRevB.91.235303 235303.
[20] V. Manivannan, R.A. Enzenroth, K.L. Barth, S. Kohli, P.R. McCurdy, W.S. Sampath, Microstructural features of cadmium telluride photovoltaic thin film devices, Thin Solid Films 516 (6) (2008) 1209–1213, https://doi.org/10.1016/j.tsf.2007.05.043.
[21] C.H. Lee, E.B. Nam, M.-E. Lee, S.U. Lee, Unraveling the controversy over a catalytic reaction mechanism using a new theoretical methodology: one probe and non-equilibrium surface Green's function, Nano Energy 63 (2019), https://doi.org/10.1016/j.nanoen.2019.103863 103863.
[22] Y. An, Y. Hou, S. Gong, R. Wu, C. Zhao, T. Wang, Z. Jiao, H. Wang, W. Liu, Evaluating the exfoliation of two-dimensional materials with a Green's function surface model, Phys. Rev. B 101 (2020), https://doi.org/10.1103/PhysRevB.101.075416 075416.
[23] M.A. Berding, S. Krishnamurthy, A. Sher, A.-B. Chen, Cleavage energies in semiconductors, J. Appl. Phys. 67 (10) (1990) 6175–6178, https://doi.org/10.1063/1.345181.
[24] J. Gordon, P. Morgen, H. Shechter, M. Folman, Adsorption of Li, Cs, and O on CdTe, Phys. Rev. B 52 (1995) 1852–1858, https://doi.org/10.1103/PhysRevB.52.1852.
[25] S. Tatarenko, F. Bassani, J.C. Klein, K. Saminadayar, J. Cibert, V.H. Etgens, Surface reconstructions of (001) CdTe and their role in the dynamics of evaporation and molecular-beam epitaxy growth, J. Vac. Sci. Technol. A 12 (1) (1994) 140–147, https://doi.org/10.1116/1.578910.
[26] K. Yong, A. Gellman, P. Sides, The structure and composition of vicinal CdTe(1 0 0) surfaces, Surf. Sci. 374 (1) (1997) 65–72, https://doi.org/10.1016/S0039-6028(96)01195-8.
[27] B. Rerbal, G. Merad, H. Mariette, H. Faraoun, J.-M. Raulot, Ab initio investigation of the CdTe (001) surface, Superlattices Microstruct. 46 (5) (2009) 733–744, https://doi.org/10.1016/j.spmi.2009.07.025.
[28] Y.S. Wu, C.R. Becker, A. Waag, K. von Schierstedt, R.N. Bicknell-Tassius, G. Landwehr, Surface sublimation of zinc blende CdTe, Appl. Phys. Lett. 62 (13) (1993) 1510–1512, https://doi.org/10.1063/1.108623.
[29] J. Li, N. Kioussis, F. Aqariden, C. Grein, Thermodynamic and stoichiometric stability of the Cd-terminated CdTe (1 1 1) surface, Phys. Rev. B 85 (2012), https://doi.org/10.1103/PhysRevB.85.235306 235306.
[30] D. Odkhuu, M.-S. Miao, F. Aqariden, C. Grein, N. Kioussis, Atomic and electronic structure of CdTe/metal (Cu, Al, Pt) interfaces and their influence to the Schottky barrier, J. Appl. Phys. 120 (18) (2016), https://doi.org/10.1063/1.4966931 185703.
[31] T. Takahashi, A. Ebina, Electronic surface states of II-VI compound semiconductors, Appl. Surf. Sci. 11–12 (1982) 268–287, https://doi.org/10.1016/0378-5963(82)90074-5.
[32] C.K. Egan, Q.Z. Jiang, A.W. Brinkman, Morphology and reconstructions of polar CdTe(1 1 1)A, B surfaces by scanning tunneling microscopy, J. Vac. Sci. Technol. A 29 (1) (2011), https://doi.org/10.1116/1.3525914 011021.
[33] S. Gundel, A. Fleszar, W. Faschinger, W. Hanke, Atomic and electronic structure of the CdTe(001) surface: LDA and GW calculations, Phys. Rev. B 59 (1999) 15261–15269, https://doi.org/10.1103/PhysRevB.59.15261.
[34] J. Li, J. Gayles, N. Kioussis, Z. Zhang, C. Grein, F. Aqariden, Ab initio studies of the unreconstructed CdTe (1 1 1) surface, J. Electron. Mater. 41 (2012) 2745–2753,

https://doi.org/10.1007/s11664-012-1924-x.
[35] S.Y. Tong, G. Xu, W.N. Mei, Vacancy-buckling model for the (2 × 2) GaAs(1 1 1) surface, Phys. Rev. Lett. 52 (1984) 1693–1696, https://doi.org/10.1103/PhysRevLett.52.1693.
[36] G. Srivastava, The electron counting rule and passivation of compound semiconductor surfaces, Appl. Surf. Sci. 252 (21) (2006) 7600–7607, https://doi.org/10.1016/j.apsusc.2006.03.076 Proceedings of the 4th International Workshop on Semiconductor Surface Passivation.
[37] A. Crovetto, M.L.N. Palsgaard, T. Gunst, T. Markussen, K. Stokbro, M. Brandbyge, O. Hansen, Interface band gap narrowing behind open circuit voltage losses in Cu2ZnSnS4 solar cells, Appl. Phys. Lett. 110 (8) (2017), https://doi.org/10.1063/1.4976830 083903.
[38] J. Fritsche, A. Klein, W. Jaegermann, Thin film solar cells: materials science at interfaces, Adv. Eng. Mater. 7 (10) (2005) 914–920, https://doi.org/10.1002/adem.200500126.
[39] A.P. Nicholson, A.H. Munshi, U.P.W.S. Sampath, First Principles Approach to CdTe/Te Interface Band Alignment Using Density Functional Theory and Nonequilibrium Green's Function, in: 2018 IEEE 7th World Conference on Photovoltaic Energy Conversion (WCPEC) (A Joint Conference of 45th IEEE PVSC, 28th PVSection 34th EU PVSEC), 2018, pp. 1932–1936, https://doi.org/10.1109/WCPEC40376.2018.
[40] R.T. Tung, Recent advances in Schottky barrier concepts, Mater. Sci. Eng. 35 (1) (2001) 1–138, https://doi.org/10.1016/S0927-796X(01)00037-7.
[41] R.L. Anderson, Experiments on Ge-GaAs heterojunctions, Solid State Electron. 5 (5) (1962) 341–351, https://doi.org/10.1016/0038-1101(62)90115-6.